# Optimum electromagnetic heating of nanoparticle thermal contrast agents at rf frequencies

George W. Hanson[1,a)] and S. K. Patch[2]

[1]*Department of Electrical Engineering, University of Wisconsin-Milwaukee, 3200 N. Cramer St., Milwaukee, Wisconsin 53211, USA*
[2]*Department of Physics, University of Wisconsin-Milwaukee, 3200 N. Cramer St., Milwaukee, Wisconsin 53211, USA*

Enhanced heating of nanoparticles for applications such as thermoacoustic imaging and therapeutic heat delivery is considered. The optimum electrical conductivity to achieve maximum electromagnetic energy deposition in a given nanoparticle is obtained, with emphasis on rf frequencies, where plasmon resonances associated with negative permittivity are generally not possible. Spheres, coated spheres, nanowires, and carbon nanotubes are considered. In all cases, it is found that relatively small conductivity values (e.g., $\sigma \ll 1$ S/m for spheres) provide the maximum absorption of rf energy, and thus maximizes heat production in the nanoparticle. Therefore, lossy dielectrics may be a better choice for maximizing nanoparticle heat production than metallic particles. © *2009 American Institute of Physics*. [doi:10.1063/1.3204653]

## I. INTRODUCTION

Nanoparticles are being widely developed as contrast agents in thermal-related medical imaging technologies, such as photoacoustic and thermoacoustic imaging.[1–3] In these imaging applications, electromagnetic energy is applied to a sample, generating heat and subsequent thermal expansion, which produces an acoustic wave that is measured by an array of acoustic sensors. Thermo- and photoacoustic imaging are therefore inverse source problems, providing completely different contrast mechanisms than traditional diagnostic imaging techniques. Differential heating in cancerous and noncancerous tissue, for example, can thereby be used to produce an image,[4–6] even without the benefit of contrast enhancement.

Typically, photoacoustics refers to irradiating the sample with electromagnetic energy in the visible regime, whereas thermoacoustics irradiates in the microwave and rf range. Thermoacoustic imaging, in particular, provides deep tissue penetration and large sampling volumes, and the imaging region is irradiated as uniformly as possible in space and as briefly as possible in time. In photoacoustics, illumination with near-infrared (NIR) pulses generates high photoacoustic signal-to-noise (S/N) because tissue is very lossy to NIR radiation. Precisely for this reason, depth penetration of photoacoustics is limited to a few centimeters. Similarly, microwave illumination efficiently heats water and provides reasonable signal levels but limited depth penetration. Therefore, for thermoacoustics we have investigated rf illumination pulses with carrier frequencies near 100 MHz.[7] Because there is less loss in tissue at these frequencies, rf excitation pulses provide good depth penetration, but low S/N. The need to boost S/N for this large imaging field of view application prompts us to study heating enhancement due to nanoparticle thermal contrast agents.

Nanoparticles are also being investigated for preferential heating of biological structures for cancer treatment.[8–11] In this case, electromagnetic energy is intended to cause localized heating of nanoparticles attached to cancer cells, or embedded in tumors, resulting in selective destruction of the diseased tissue.

In both thermotherapy and thermo/photoacoustic imaging applications, efficient heating of nanoparticles is important. In this regard, various thermal contrast agents have been utilized in measurements, where here we define contrast agent as a particle added to a sample to increase heating, either in an imaging modality or in a therapeutic application. The main classes of particles that have been investigated are carbon nanotubes (CNs)[2,9,12] and metallic (gold) nanospheres.[8,10,11] In particular, both gold nanospheres and CNs have been shown to greatly enhance tissue heating upon the application of quasisteady state rf energy (after tens to hundreds of seconds). On the theoretical side, there has not been much analysis of this heating. The size, shape, and material composition of nanoparticles that lead to maximum heating at rf frequencies has not been investigated, although there has been work done at optical frequencies via plasmon resonances.[13,14]

To heat a particle with electromagnetic energy it is clear that the particle must have some (perhaps effective) conductivity. By effective conductivity, we mean that in a description of the material permittivity $\varepsilon = \varepsilon' - j\varepsilon'' = (\varepsilon_r' - j\sigma/\omega\varepsilon_0)\varepsilon_0$ all loss mechanisms are described by finite, nonzero $\varepsilon''$, associated with $\sigma$, regardless of the nature of the loss (conduction, dipolar friction, etc.). Clearly, in the extreme limit of perfect conductivity ($\varepsilon'', \sigma \rightarrow \infty$) the material will not heat, since there is no loss mechanism. In the opposite extreme limit of zero conductivity ($\varepsilon'', \sigma \rightarrow 0$) there will also be no loss and no heating. However, *a priori* it is not clear what may be the optimum value of $\sigma$ or $\varepsilon''$ that maximizes heating for a given particle shape. In this work, we (1) investigate what is the optimum material $\sigma$ or $\varepsilon''$ for several nanoparticle

a)Electronic mail: george@uwm.edu.

shapes of interest and (2) discuss the resulting energy dissipation and heating produced by these nanoparticles. We find that for nanoradius, electrically long cylinders at rf frequencies, the best possible theoretical conductivity to maximize dissipation is very large, far above what is possible with gold ($\sigma \sim 10^7$ S/m). This is a skin effect issue, and the optimum value of skin depth ($\delta$) to maximize dissipation is found to be $\delta/a \sim 3$, where $a$ is radius. For electrically small objects such as electrically short cylinders and small spheres, the best possible theoretical conductivity to maximize dissipation is very small, typically $\sigma \ll 100$ S/m for cylinders, and $\sigma \ll 1$ S/m for spheres. The reason for this is screening of the incident field by induced charge on the finite structures; higher conductivity leads to stronger screening, and thus less internal dissipation. For an electrically long cylinder with electric field parallel to its axis, this screening charge is not present, and the problem is governed by skin effect.

In what follows, we restrict attention to electrical and thermal steady state and isotropic mediums. All units are SI and the time dependence is $e^{j\omega t}$. Most numerical results are presented at 10 MHz, since this is the frequency used in some recent papers on rf nanoparticle heating.[8–12]

## II. ENERGY DEPOSITION IN CYLINDERS AND SPHERES

Energy deposition in a material is governed by Poynting's theorem, and for time-harmonic fields[15,16]

$$-\int_{\partial\Omega} \frac{1}{2}\mathrm{Re}(\mathbf{E}\times\mathbf{H}^*)\cdot d\mathbf{S} = \int_{\Omega}\frac{1}{2}\mathrm{Re}(\mathbf{E}\cdot\mathbf{J}^*)dr^3, \quad (1)$$

where the first term is the power into the volume $\Omega$ bounded by surface $\partial\Omega$, and the second term is the power dissipated by the field as heat in $\Omega$. Using $\mathbf{J}=\sigma\mathbf{E}$, the power density (W/m$^3$) is

$$S = \frac{1}{2}\mathrm{Re}(\sigma^*\mathbf{E}\cdot\mathbf{E}^*) = \frac{1}{2}\mathrm{Re}(\sigma^*)|\mathbf{E}|^2. \quad (2)$$

Material permittivity is given as

$$\varepsilon = \left(\varepsilon_r - j\frac{\sigma}{\omega\varepsilon_0}\right)\varepsilon_0 = (\varepsilon' - j\varepsilon'')\varepsilon_0, \quad (3)$$

where $\varepsilon_r = \varepsilon'$ is real valued and accounts for all polarization mechanisms and $\sigma/\omega\varepsilon_0 = \varepsilon''$ is real valued and accounts for all loss mechanisms. In this way, $\mathbf{J}=\sigma\mathbf{E}$ is a generalized current, accounting for both conduction and polarization losses. Therefore, we have simply

$$S = \frac{1}{2}\sigma|\mathbf{E}|^2 = \frac{1}{2}\omega\varepsilon_0\varepsilon''|\mathbf{E}|^2. \quad (4)$$

Assuming conduction as the dominant heat transfer mechanism, this is the term that enters the steady-state heat (Poisson) equation,

$$k_m\nabla^2 T(\mathbf{r}) + S(\mathbf{r}) = 0, \quad (5)$$

where $k_m$ is the thermal conductivity (W/mK).

### A. Electrically long solid cylinder

We consider an infinite material cylinder as a model of an electrically long cylinder $k_h L \gg 1$, where $L$ is wire length and $k_h$ is the wave number in the host medium of the cylinder. Although at rf frequencies long wires are not of much interest in thermocontrast applications, they may be of use above gigahertz frequencies where physical lengths can be quite short. Also, importantly, they provide a striking contrast to the behavior found for short wires and nanoparticles, as explained in the Introduction and in Secs. II C–II E.

For an infinite material cylinder oriented along the $z$ axis, having complex permittivity $\varepsilon_d$ and radius $a$, immersed in a host medium having complex permittivity $\varepsilon_h$, the field inside the cylinder due to an incident plane wave $\mathbf{E}^i(\mathbf{r}) = \hat{\mathbf{z}}E_0 e^{-jk_h x}$ is[17]

$$\mathbf{E}^d(r) = \hat{\mathbf{z}}E_0 \sum_{n=-\infty}^{\infty} j^{-n}b_n J_n(k_d r)e^{jn\phi}, \quad (6)$$

where

$$b_n = \frac{J_n(k_h a)H_n^{(2)\prime}(k_h a) - J_n'(k_h a)H_n^{(2)}(k_h a)}{J_n(k_d a)H_n^{(2)\prime}(k_h a) - \sqrt{\varepsilon_d/\varepsilon_h}J_n'(k_d a)H_n^{(2)}(k_h a)}, \quad (7)$$

and where $k_d = \omega\sqrt{\mu_0\varepsilon_d}$ is the wave number in the cylinder and $k_h = \omega\sqrt{\mu_0\varepsilon_h}$ is the wave number in the host region. This result is exact, and the power density can be computed from Eq. (2) or (4).

For a small radius cylinder, assuming $k_h a, k_d a \ll 1$, $\mathbf{E}^d(r) \simeq \hat{\mathbf{z}}E_0 b_0 J_0(k_d r)$. The current density is $\mathbf{J}(r) = \hat{\mathbf{z}}\sigma E_0 b_0 J_0(k_d r)$ and the current carried by the cylinder is

$$I = \sigma E_0 b_0 \int_0^{2\pi}\int_0^a J_0(k_d r)r\,dr\,d\phi = E_0\frac{2\pi a\sigma}{k_d}b_0 J_1(k_d a).$$

If we assume a metallic cylinder with $\varepsilon_d = (\varepsilon_d' - j\sigma/\omega\varepsilon_0) \simeq -j\sigma/\omega\varepsilon_0$, then $k_d \simeq e^{-j\pi/4}\sqrt{\sigma\omega\mu_0}$ and

$$I = E_0 2\pi a\sqrt{\frac{\sigma}{\omega\mu_0}}e^{j\pi/4}b_0 J_1(e^{-j\pi/4}\sqrt{\sigma\omega\mu_0}a). \quad (8)$$

With $R' = 1/\pi a^2\sigma$ $\Omega$/m (assuming $\delta/a > 1$, where $\delta = \sqrt{2/\omega\mu_0\sigma}$ is the skin depth,[16] the current is nearly uniformly distributed through the wire and this expression is valid),

$$Q' = \frac{1}{2}\sigma|\mathbf{E}|^2(\pi a^2) = \frac{1}{2}|I|^2 R'$$

$$= \frac{1}{2}|E_0|^2\frac{4\pi}{\omega\mu_0}|b_0|^2|J_1(e^{-j\pi/4}\sqrt{\sigma\omega\mu_0}a)|^2, \quad (9)$$

where the units of $Q'$ are W/m.

To determine the condition for maximum heating, we set $dQ'/d\sigma = 0$. Using

$$b_0 \simeq \frac{1}{1 + \left(\dfrac{\pi a^2\omega\mu_0\sigma}{4}\right)\left[1 - j\dfrac{2}{\pi}\ln\left(\dfrac{k_h a}{2}\right)\right]}, \quad (10)$$

we obtain the value of conductivity the leads to maximum dissipation/heat production as,

$$\sigma_{\max}^{\text{lc}} = \frac{2}{\omega\mu_0 a^2 |\ln(k_h a)|}, \tag{11}$$

where the superscript indicates that this is the long cylinder result. This will give maximum heating for a small radius, electrically long material cylinder. It is useful to consider this value in terms of skin depth,

$$\left(\frac{\delta}{a}\right)_{\max} = \sqrt{|\ln(k_h a)|}. \tag{12}$$

For a wire in water ($\varepsilon_h = 70$), for $f = 10$ MHz and $a = 100$ nm, $k_h a = 2.096 \times 10^{-8}$ and $(\delta/a)_{\max} = 3.94$ from Eq. (12). Setting the derivative of the exact expression [from Eq. (6)] equal to zero and performing numerical differentiation to obtain the value of $\delta/a$ that maximizes power absorption yields $\delta/a = 4.0$, close to the approximate value. For $a = 50$ nm, the approximate expression yields $(\delta/a)_{\max} = 4.03$, and the numerical computation results in $\delta/a = 4.09$. Moreover, at $f = 10$ GHz and $a = 100$ nm, the approximate expression (12) yields $(\delta/a)_{\max} = 2.94$, while the numerical computation results in $\delta/a = 3.03$. Thus, it is found that Eqs. (11) and (12) provide a very good approximation for the value of conductivity and skin depth that maximizes absorption. Numerically, the optimum skin depth is found to be $\delta/a \sim 2-4$, even when the cylinder does not have a very small radius (say, $k_h a \ll 1$, $k_d a > 1$).

Under conditions of maximum absorption, using Eq. (12) and setting $\delta/a = 3$ with $b_0 \simeq 1/(1+j)$,

$$Q'_{\max} = \frac{1}{2}|E_0|^2 \frac{2\pi}{\omega\mu_0} \left| J_1\left( \sqrt{\frac{2}{|\ln(k_h a)|}} e^{-j\pi/4} \right) \right|^2. \tag{13}$$

With $|\ln(k_h a)| = 9$ and $|J_1|^2 = 0.056$,

$$Q'_{\max} = |E_0|^2 \frac{0.056\pi}{\omega\mu_0}. \tag{14}$$

For an electrically long cylinder, the current on the cylinder $I(z)$ due to an incident plane wave is approximately the same as the current on an infinite-length cylinder, except that for the finite-length case current goes to zero at the cylinder ends. Total power dissipated ($W$) can be obtained simply as

$$Q = Q'L, \tag{15}$$

where $Q'$ is Eq. (9) and $L$ is the cylinder length. One can define an absorption cross section $C_a^{\text{cyl}}(m^2)$ for the electrically long cylinder as

$$Q = C_a^{\text{cyl}} I_a, \tag{16}$$

where $I_a = |\mathbf{E}|^2 / 2\eta$ is the intensity of the incident electromagnetic wave, and $\eta = \sqrt{\mu_h/\varepsilon_h}$. From Eq. (14),

$$C_a^{\text{cyl,max}} = 2\eta \frac{0.056\pi}{\omega\mu_0} L. \tag{17}$$

Unfortunately, for nanoradius electrically long cylinders achieving $\sigma_{\max}^{\text{lc}}$ at rf is impossible except for moderately high frequencies. Let $\sigma_{\max} = \alpha_{\max}\sigma_0$, where $\sigma_0 = 4.6 \times 10^7$ S/m is the conductivity of gold. Then,

$$\alpha_{\max} = \frac{1}{f_{\text{GHz}} a_{\text{nm}}^2} \left( \frac{2.07 \times 10^3}{\delta/a} \right)^2 = \frac{4.76 \times 10^5}{f_{\text{GHz}} a_{\text{nm}}^2}, \tag{18}$$

using $\delta/a = 3$, where $f_{\text{GHz}}$ is the frequency in gigahertz and $a_{\text{nm}}$ is the radius in nanometers. If $a_{\text{nm}} = 10^3$, then $\alpha = 0.614/f_{\text{GHz}}$; a less conductive material than gold is optimum above 614 MHz, whereas below this frequency we would ideally use a better conductor. At a fixed frequency, as radius decreases conductivity must increase to obtain maximum heat generation. Assuming $a = 100$ nm, one needs to be above 47.6 GHz to be able to achieve the theoretically maximum heat production using realistic materials. Below 47.6 GHz, the best that one can do is to use the material with the highest possible conductivity. In general, when $a$ is extremely small at rf frequencies, power absorption is given by

$$\frac{1}{2}|I|^2 R' \simeq \frac{1}{2}|E_0|^2 \frac{\pi a^2 \sigma}{\frac{1}{4}a^4(\omega\mu_0\sigma)^2 \ln^2(k_h a) + 1}, \tag{19}$$

$$\simeq \frac{1}{2}|E_0|^2 \pi a^2 \sigma, \tag{20}$$

independent of frequency. In this case, power dissipation is increased as either $\sigma$ or $a$ is increased.

## B. Arbitrary length solid cylinder

The previous analysis assumed an electrically long solid cylinder, which practically means $k_h L \gg 1$. Those results were verified by solving the Hallén integral equation for wire current $I(z)$ on an arbitrary-length electrically thin ($k_h a \ll 1$) wire,[18–20]

$$\int_{-L/2}^{L/2} [K(z-z') + q(z-z')]I(z')dz' = c_1 \sin k_h z$$
$$+ c_2 \cos k_h z - \frac{j4\pi}{\eta} \int_0^z E_z^i(z')\sin[k_h(z-z')]dz', \tag{21}$$

for $-L/2 \le z \le L/2$, where $E_z^i$ is the incident electric field parallel to the wire, $L$ is the wire length, and $c_{1,2}$ are unknown constants,

$$K(z-z') = \frac{1}{2\pi} \int_{-\pi}^{\pi} \frac{e^{-jk_h\sqrt{(z-z')^2 + 4a^2\sin^2(\phi'/2)}}}{\sqrt{(z-z')^2 + 4a^2\sin^2(\phi'/2)}} d\phi', \tag{22}$$

$$q(z-z') = 2\pi\omega\varepsilon_0 z_s \frac{e^{-jk_h|z-z'|}}{k_h}, \tag{23}$$

and $z_s$ is the surface impedance ($\Omega/m$) (Ref. 21) (valid if $\sigma/\omega\varepsilon_0 \gg 1$),

$$z_s = \frac{\gamma J_0(\gamma a)}{2\pi a\sigma J_1(\gamma a)}, \tag{24}$$

where $\gamma = (1-j)\sqrt{\omega\mu_0\sigma/2}$. Integral equation (21) was solved using a rectangular pulse function expansion, point testing solution.[22] Power absorbed was computed as

$$Q = \frac{1}{2}\text{Re}(z_s)\int_{-L/2}^{L/2}|I(z)|^2 dz, \tag{25}$$

which was compared to Eq. (15) for long wires and good agreement was found (note that $\text{Re}(z_s) \simeq 1/\pi a^2 \sigma = R'$ when $k_h a \ll 1$).

Therefore, for long thin cylinders the simple analytical solution (9) can be used to compute power absorbed via Eq. (15). For cylinder lengths near $k_h L = 1$, the integral equation, or another full wave method (e.g., FDTD, FEM) must be used. However, these resonant length cylinders are not of much interest for thermoapplications at rf frequencies since the wires will be physically very long. Our main reason for presenting the integral equation is that it can be used to verify the important small cylinder case ($k_h L \ll 1$) discussed next, and to help understand why maximum heating for small objects requires very different conductivity values than for long wires.

## C. Electrically short solid cylinder

For a cylinder having $k_h a, k_h L \ll 1$, the response will be dominated by the dipole moment of the cylinder, and we can use the concept of polarizabilities.[23] In this case, the absorption cross section (m$^2$) for an electrically small object, assuming that the background material is lossless, is

$$C_a = -k_h \,\text{Im}(\alpha), \tag{26}$$

where $\alpha$ is the polarizability (m$^3$) and $k_h$ is the wave number in the background/host medium. Although in practice the host medium may be lossy too, as a first approximation we neglect direct host medium heating, and concentrate on the effect of the nanoparticle, since in this case we obtain simple expressions for $\sigma_{max}$.

For a prolate spheroid in the needle limit, as a good approximation of a cylinder,[23]

$$C_a^{cyl} = -k_h 4\pi\frac{La^2}{6}\text{Im}\left[\frac{\varepsilon_d - \varepsilon_h}{\varepsilon_h + L_d(\varepsilon_d - \varepsilon_h)}\right], \tag{27}$$

where $\varepsilon_h$ and $\varepsilon_d$ are the again permittivities of the host and cylinder materials, respectively, and where the geometrical depolarization factor is

$$L_d = \frac{1-e^2}{e^2}\left[-1 + \frac{1}{2e}\ln\left(\frac{1+e}{1-e}\right)\right], \quad e^2 = 1 - \frac{a^2}{(L/2)^2} \tag{28}$$

($e$ is the eccentricity). The power dissipated in the cylinder is

$$Q = C_a^{cyl}I_a, \tag{29}$$

where $I_a$ is the intensity of the incoming wave. For wires short enough to be modeled by their polarizability, power computed by Eq. (29) was found to be in good agreement to that computed from the integral equation (21) using Eq. (25).

The value of conductivity that maximizes absorbed power $\sigma_{max}$ is obtained from $dC_a^{cyl}/d\sigma = 0$, leading to

$$\sigma_{max}^{sc} = [(1-L_d)\varepsilon_h + \varepsilon_d' L_d]\frac{\omega\varepsilon_0}{L_d}, \tag{30}$$

where the superscript indicates that this is the short cylinder result and $\varepsilon_d'$ is the real part of the relative cylinder permit-
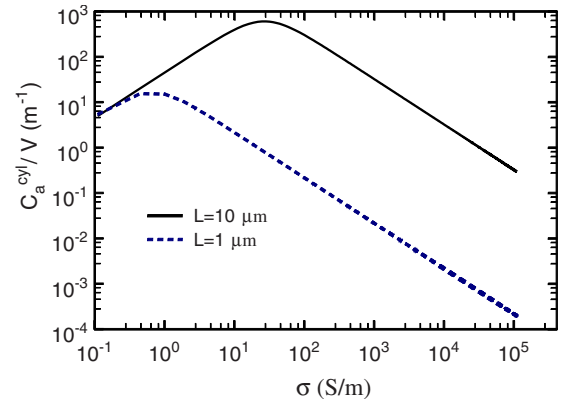


FIG. 1. (Color online) Absorption cross section (27) of a prolate spheroid model of a short cylinder, normalized by particle volume, as a function of conductivity at $f = 10$ MHz, $a = 100$ nm, and $\varepsilon_h = 70$, for two values of cylinder length $L$.

tivity. At this value of conductivity the absorption cross section is maximized,

$$C_a^{cyl,max} = -k_h 2\pi\frac{La^2}{3}\left(\frac{\varepsilon_h}{L_d^2(\varepsilon_h - \varepsilon_d') - L_d\varepsilon_h}\right). \tag{31}$$

For $f = 10$ MHz, $L = 10$ $\mu$m, and $a = 100$ nm, $\sigma_{max}^{sc} = 0.385$ S/m and $C_a^{cyl,max} = 1.5 \times 10^{-17}$ m$^2$ for the host material being air, and, if the host material is water, assuming $\varepsilon_h = 70$, $\sigma_{max}^{sc} = 26.9$ S/m and $C_a^{cyl,max} = 1.3 \times 10^{-16}$ m$^2$. For $L = 1$ $\mu$m and $a = 100$ nm, assuming $\varepsilon_h = 70$, $\sigma_{max}^{sc} = 0.659$ S/m and $C_a^{cyl,max} = 3.5 \times 10^{-19}$ m$^2$. Whereas for the infinite length cylinder we can maximize dissipation when $\delta/a \sim 3$, for the $L = 10$ $\mu$m wire with $\sigma = \sigma_{max}^{sc} = 26.9$ S/m, the corresponding skin depth is $\delta/a = 3.1 \times 10^5$.

Note the dramatic difference between the electrically long and electrically short cylinder cases, $\sigma_{max}^{lc}$ and $\sigma_{max}^{sc}$. For an air host medium with $f = 10$ MHz and $a = 100$ nm, $\sigma_{max}^{lc} = 1.4 \times 10^{11}$ S/m, an unattainable value, whereas for a short wire having $L = 10$ $\mu$m, $\sigma_{max}^{sc} = 0.386$ S/m, a difference of eleven orders of magnitude This has been verified using integral equation (21), which can be considered to be an independent method (it is not based on polarizabilities, and it does not involve any assumptions other than that the wire is thin, $k_h a \ll 1$ and $L/a \gg 1$). As explained in the introduction, the huge difference in the values of $\sigma_{max}^{lc}$ and $\sigma_{max}^{sc}$ is due to screening of the incident field by induced charge. Higher conductivity would lead to stronger screening and less dissipation, an effect which is absent for the electrically long cylinder. From another viewpoint, for an electrically long cylinder the current due to an external plane wave is approximately constant along the structure, except for vanishing at the cylinder ends. As cylinder length is reduced, current magnitude tends to diminish and the current profile becomes one-half of a sinusoid. Since $Q' = |I|^2 R'/2$, as current diminishes $Q'$ rapidly decreases unless $R'$ increases, and so $\sigma$ must decrease to achieve maximum power absorption. This has been verified using integral equation (21).

Figure 1 shows the absorption cross section from Eq. (27) of a short cylinder normalized by particle volume ($V = 4\pi a^2 L/6$ for a spheroid with semiaxes $a, a, L/2$) as a function of conductivity at $f = 10$ MHz, $a = 100$ nm, and $\varepsilon_h = 70$,
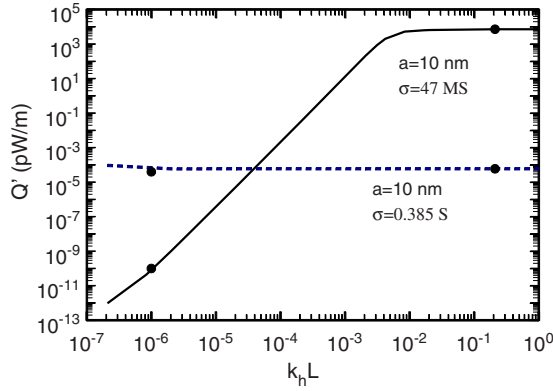
FIG. 2. (Color online) $Q'=Q/L$ (pW/m) from Eq. (21) for an $a=10$ nm radius cylinder for two values of conductivity, $\sigma=4.7\times10^7$ S/m (gold) and $\sigma=0.385$ S/m, $E_0^i=1$ V/m, and $\varepsilon_h=1$. The dots on the right side of the curves are the values predicted by the simple infinite-cylinder model (9) and those on the left side are the predictions based on the prolate spheroid model of a short cylinder [Eq. (27)].

for two values of cylinder length $L$. For comparison, a 1 $\mu$m long gold cylinder has $C_a^{\text{cyl}}/V=6.4\times10^{-7}$ m$^{-1}$.

Figure 2 shows $Q'=Q/L$ (pW/m) determined from integral equation (21) for an $a=10$ nm radius cylinder for two values of conductivity, $\sigma=4.7\times10^7$ S/m (gold), and $\sigma=0.385$ S/m, the optimum conductivity from Eq. (30) for a 1 $\mu$m long cylinder. In both cases we assume $E_0^i=1$ V/m and $\varepsilon_h=1$. For electrically short cylinders, the low-conductivity cylinder is many orders of magnitude better at dissipating energy than the gold cylinder, as expected, and for long cylinders the gold cylinder is superior. The dots on the right side of the curves are the values predicted by the simple infinite-cylinder model (9) and the dots on the left side are the predictions of the electrically short cylinder model based on a prolate spheroid [Eq. (27)]. The speed of wave propagation on a nanoradius conductor is much slower than on a macroscale conductor,[24] which is why the knee of the curve occurs for relatively small values of $k_hL$.

### D. Small material sphere

For a general material sphere the exact extinction and scattering cross sections are[23]

$$C_{\text{ext}}=\frac{2\pi}{k_h^2}\sum_{n=1}^{\infty}(2n+1)\text{Re}(a_n+b_n), \quad (32)$$

$$C_{\text{sca}}=\frac{2\pi}{k_h^2}\sum_{n=1}^{\infty}(2n+1)(|a_n|^2+|b_n|^2), \quad (33)$$

where $a_n$ and $b_n$ are the Mie coefficients, representing electric and magnetic multipoles, and the absorption cross section is $C_a=C_{\text{ext}}-C_{\text{sca}}$. For a small sphere of radius $a$ ($k_ha, k_da\ll1$) and permittivity $\varepsilon_d$, immersed in a host material having real-valued permittivity $\varepsilon_h$, the leading terms are, to order $(k_ha)^5$,

$$a_1=j\frac{2(k_ha)^3}{3}\frac{\varepsilon_d-\varepsilon_h}{\varepsilon_d+2\varepsilon_h}+j\frac{2(k_ha)^5}{5}\frac{(\varepsilon_d-2\varepsilon_h)(\varepsilon_d-\varepsilon_h)}{(\varepsilon_d+2\varepsilon_h)^2}$$

$$(34)$$

$$b_1=j\frac{(k_ha)^5}{45}\left(\frac{\varepsilon_d-\varepsilon_h}{\varepsilon_h}\right). \quad (35)$$

For small spheres the leading term in $a_1$ will be strongly dominant compared to the other terms, as well as compared to $b_1$, unless $|\varepsilon_d/\varepsilon_h|\gg1$ (i.e., a very good conductor at low frequencies), in which case $b_1$ can dominate over $a_1$ despite the factor of $(k_ha)^5$.

For very small material spheres we can ignore scattering compared to extinction, so that

$$C_a^{\text{sph}}=\frac{6\pi}{k_h^2}\text{Re}(a_1+b_1)$$

$$=-k_h\,\text{Im}\left[4\pi a^3\frac{\varepsilon_d-\varepsilon_h}{\varepsilon_d+2\varepsilon_h}+\frac{2\pi k_h^2 a^5}{15}\left(\frac{\varepsilon_d-\varepsilon_h}{\varepsilon_h}\right)\right]$$

$$=-k_h\,\text{Im}(\alpha^e+\alpha^m)=C_a^{e,\text{sph}}+C_a^{m,\text{sph}}, \quad (36)$$

where $\alpha^e$ is the electric dipole polarizability and $\alpha^m$ is the magnetic dipole polarizability[25] (associated with eddy currents).

For a small material sphere the usual plasmon resonance is $\varepsilon_d=-2\varepsilon_h$, at which point $\alpha^e\to\infty$. In practice, we can assume that $\varepsilon_d=-2\varepsilon_h+i\varsigma$, where $\varsigma\ll1$, so that for a plasmon resonance $C_a^{e,\text{sph,plasmon}}=-k_h4\pi a^3 3\varepsilon_h/\varsigma$.

However, at rf frequencies it is difficult to achieve negative permittivity values, and so we seek to maximize the absorption cross section with low conductivity. Setting $dC_a^{\text{sph}}/d\sigma\simeq dC_a^{e,\text{sph}}/d\sigma=0$ leads to

$$\sigma_{\text{max}}^{\text{sph}}=(\varepsilon_d'+2\varepsilon_h)\omega\varepsilon_0, \quad (37)$$

independent of radius. Since $\omega\varepsilon_0\ll1$ below 1 GHz, at these frequencies $\sigma_{\text{max}}^{\text{sph}}\ll1$. As a special case, if we assume $\varepsilon_d'=\varepsilon_h=1$, then the value of complex permittivity that maximizes heat production is $\varepsilon_d=1-i3$ (compared to the case of a plasmon resonance, where we would need $\varepsilon_d=-2$).

The maximum cross section assuming Eq. (37) is

$$C_a^{\text{sph,max}}\simeq C_a^{e,\text{sph,max}}=\frac{6\pi k_h a^3\varepsilon_h}{2\varepsilon_h+\varepsilon_d'}=\frac{9}{2}\frac{k_h\varepsilon_h}{2\varepsilon_h+\varepsilon_d'}V, \quad (38)$$

where $V$ is the particle volume. For $f=10$ MHz, $a=100$ nm, $\varepsilon_d'=1$, and $\varepsilon_h=70$, $\sigma_{\text{max}}^{\text{sph}}=0.078$ S/m, and $C_a^{\text{sph,max}}=1.6\times10^{-20}$ m$^2$ (strongly dominated by the electric dipole contribution). Note that, assuming $\sigma=4.6\times10^7$ S/m for gold, $C_a^{\text{sph}}=2.67\times10^{-26}$ m$^2$ (dominated by a factor of $10^3$ by the magnetic dipole contribution). Both cross sections were checked by comparing with the full Mie solutions (32) and (33). Thus, one can generate $10^6$ times more heat energy using nanospheres with an appropriately chosen value of conductivity $\sigma=\sigma_{\text{max}}^{\text{sph}}$ compared to using gold.

Figure 3 shows the absorption cross section from Eq. (36) normalized by particle volume as a function of conductivity at $f=10$ MHz, with $\varepsilon_h=70$. For these values of $\sigma$ the electric dipole term dominates, and the result is independent of particle size (assuming $k_ha, k_da\ll1$). Away from the value $\sigma=\sigma_{\text{max}}^{\text{sph}}$ the normalized cross section shows a linear behavior on a log-log scale. As a comparison, for an $a=100$ nm gold sphere, $C_a^{\text{sph}}/V=6.4\times10^{-6}$ m$^{-1}$.
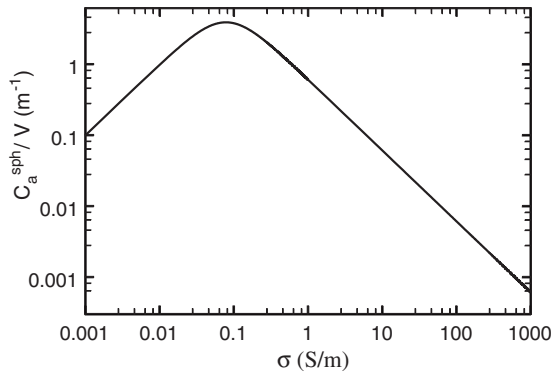
FIG. 3. Absorption cross section (36) for a small sphere ($k_h a, k_d a \ll 1$) normalized by particle volume as a function of conductivity at $f = 10$ MHz, with $\varepsilon_h = 70$.

### E. Small coated sphere

In many instances nanoparticles may have a coating, such as an oxide layer or a protein for selective binding to a cell. For a sphere having radius $a$ and permittivity $\varepsilon_d$, with a coating having thickness $d$ and permittivity $\varepsilon_{coat}$, embedded in a host medium having real-valued permittivity $\varepsilon_h$, the electric polarizability is[23]

$$\alpha^{e,cs} = 4\pi(a+d)^3$$
$$\times \frac{(\varepsilon_{coat} - \varepsilon_h)(\varepsilon_d + 2\varepsilon_{coat}) + f_c(\varepsilon_d - \varepsilon_{coat})(\varepsilon_h + 2\varepsilon_{coat})}{(\varepsilon_{coat} + 2\varepsilon_h)(\varepsilon_d + 2\varepsilon_{coat}) + f_c(2\varepsilon_{coat} - 2\varepsilon_h)(\varepsilon_d - \varepsilon_{coat})},$$
$$(39)$$

where $f_c = [a/(a+d)]^3$. Even if the core is a good metal, the presence of an absorptive coating generally causes the electric dipole contribution to be large compared to the magnetic dipole contribution, as can be verified numerically using the Mie coefficients for the coated sphere.[23]

The presence of even a very thin absorbing coating can have a profound influence on the absorbing properties of the particle.[38] For example, let the host medium be water with $\varepsilon_h = 70$, and assume that the inner sphere is gold. Then, for $f = 10$ MHz and $a = 100$ nm, the uncoated sphere has an absorption cross section of $2.67 \times 10^{-26}$ m². If we add a coating with $d = 0.01a$ ($f_c = 0.971$), $\varepsilon'_{coat} = 10$ and $\sigma = 0.001$ S/m, the absorption cross section becomes $6.4 \times 10^{-22}$ m², an increase in $10^4$ for a coating that is 1% of the gold sphere's radius.

If $|\varepsilon_d| \gg |\varepsilon_{coat}|$, then the value of coating conductivity that maximizes the absorption cross section is

$$\sigma_{max}^{cs} = \omega\varepsilon_0\left(\varepsilon'_{coat} + 2\varepsilon_h \frac{1 - f_c}{1 + 2f_c}\right), \quad (40)$$

assuming $f_c \neq 1$. At 10 MHz, for a gold sphere having $a = 100$ nm with a coating $d = 0.01a$, $\varepsilon'_{coat} = 10$, and $\varepsilon_h = 70$, then $\sigma_{max}^{cs} = 0.0063$ S/m, and $C_a^{cs} = 2.1 \times 10^{-21}$ m², an increase by a factor of $10^5$ compared to the uncoated gold sphere. For comparison, from Eq. (38) for an optimized uncoated sphere having $\sigma = \sigma_{max}^{sph}$, $C_a^{sph,max} = 1.6 \times 10^{-20}$ m². Therefore, surprisingly for this extremely thin coating, an optimized, uncoated dielectric nanosphere is only a factor of 10 better than an optimized, thinly coated gold sphere.
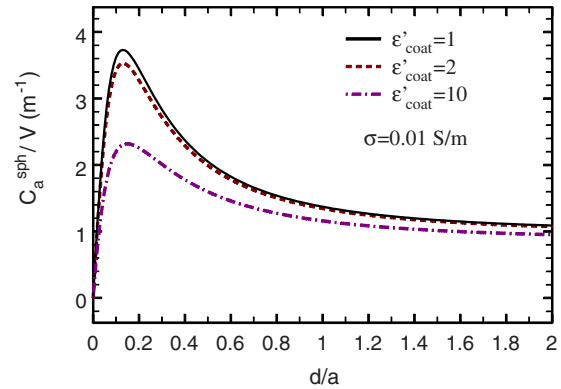


FIG. 4. (Color online) Normalized absorption cross section of a gold sphere coated with lossy dielectric vs $d/a$, for $a = 100$ nm, $\varepsilon_h = 70$, $f = 10$ MHz, $\sigma = 0.01$ S/m, for several values of coating permittivity $\varepsilon'_{coat}$

Figure 4 shows the normalized absorption cross section $C_a^{cs} = -k_h \operatorname{Im}(\alpha^{e,cs})$ of a gold sphere coated with lossy dielectric versus $d/a$, for $a = 100$ nm, $\varepsilon_h = 70$, $f = 10$ MHz, $\sigma = 0.01$ S/m, for several values of coating permittivity $\varepsilon'_{coat}$. It can be seen that lower permittivity leads to a larger cross section. As the coating becomes thick, the ideal conductivity that maximizes the absorption cross section tends to a constant,

$$\sigma_{max}^{cs}|_{d \to \infty} = \omega\varepsilon_0(\varepsilon'_{coat} + 2\varepsilon_h). \quad (41)$$

Figure 5 shows the normalized absorption cross section of a gold sphere coated with lossy dielectric versus $d/a$, for $a = 100$ nm, $\varepsilon_h = 70$, $f = 10$ MHz, and the real part of coating permittivity $\varepsilon'_{coat} = 1$, for several values of coating conductivity. For a given coating complex permittivity, an optimum value of thickness can be found, and, conversely, for a fixed coating thickness, an optimum conductivity can be found.

### F. Electrically long single wall CN

As a model of an electrically long single wall CN (SWCNT), the field scattered by an infinite-length CN is[26]

$$E_z^s = E_0 \frac{-\eta_h \sigma_{cn} J_0^2(k_h a)}{\frac{2}{\pi k_h a} + \eta_h \sigma_{cn} H_0^{(2)}(k_h a) J_0(k_h a)} H_0^{(2)}(k_h a), \quad (42)$$
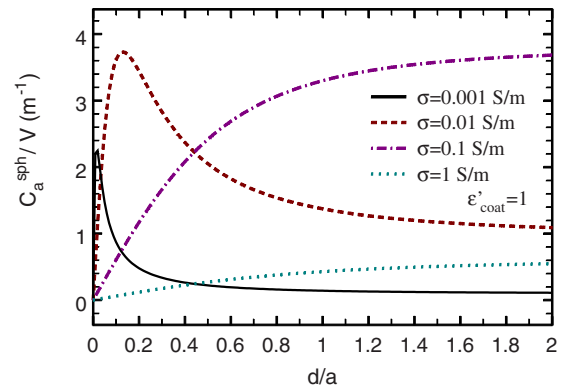


FIG. 5. (Color online) Normalized absorption cross section of a coated sphere vs $d/a$, for $a = 100$ nm, $\varepsilon_h = 70$, $f = 10$ MHz, and the real part of coating permittivity $\varepsilon'_{coat} = 1$, for several values of coating conductivity.

$$= E_0 Y H_0^{(2)}(k_h a), \tag{43}$$

where $\eta_h = \sqrt{\mu_h / \varepsilon_h}$ (we assume the same environment outside and inside the tube). The current is

$$I = 2\pi a \sigma_{cn} E_0 [1 + Y H_0^{(2)}(k_h a)] \simeq 2\pi a \sigma_{cn} E_0, \tag{44}$$

and we obtain

$$Q' = \frac{1}{2} |I|^2 R'_{cn}, \tag{45}$$

where

$$R'_{cn} = \frac{1}{2\pi a \, \mathrm{Re}(\sigma_{cn})}. \tag{46}$$

For a long but finite-length tube, $Q \simeq Q'L$.

The nanotube conductivity for armchair and zigzag tubes can be obtained from[27,28]

$$\sigma_{cn}(\omega) = \frac{je^2}{\pi^2 \hbar a} \frac{1}{(\omega - j\nu)} \sum_{s=1}^{m} \int_{1stBZ} \frac{\partial F_c}{\partial p_z} \frac{\partial \mathcal{E}_c}{\partial p_z} dp_z, \tag{47}$$

where $e$ is the charge of an electron, $\nu = \tau^{-1}$ is the phenomenological relaxation frequency, $\hbar$ is the reduced Planck's constant, $p_z$ is the quasimomentum in the longitudinal direction, and $F_c = (1 + e^{[\varepsilon_c / k_B T]})^{-1}$ is the equilibrium Fermi distribution function, in which $T$ is the temperature in kelvin, and $k_B$ is Boltzmann's constant. In Eq. (47), the electron dispersion relation is

$$\mathcal{E}_c(p_z, s) = \gamma_0 \sqrt{1 + 4\cos(\xi_z^a)\cos(\xi_s) + 4\cos^2(\xi_s)}, \tag{48}$$

for zigzag CNs, and

$$\mathcal{E}_c(p_z, s) = \gamma_0 \sqrt{1 + 4\cos(\xi_z^b)\cos(\xi_s) + 4\cos^2(\xi_z^b)}, \tag{49}$$

for armchair CNs, where $\xi_z^a = 3bp_z/(2\hbar)$, $\xi_z^b = \sqrt{3}bp_z/(2\hbar)$, and $\xi_s = \pi s/m$, and where $s = 1, 2, \ldots, m$ accounts for the quantized momentum in the circumferential direction, with $\gamma_0 \approx 2.5 - 3.1$ eV being the approximate range of the overlap integral.

In the limit of metallic tubes having small radius,[27,28]

$$\sigma_{sr}(\omega) \simeq \frac{2e^2 v_F \tau}{\pi^2 \hbar a(1 + j\omega\tau)} = \frac{\sigma_0^{sr}}{(1 + j\omega\tau)}, \tag{50}$$

where $v_F \simeq 9.71 \times 10^5$ m/s is the Fermi velocity, and for large radius tubes (metallic or semiconducting) the conductivity becomes that of graphene,

$$\sigma_{lr}(\omega) = \frac{\tau e^2 2 \ln(2) k_B T}{\pi \hbar^2 (1 + j\omega\tau)} = \frac{\sigma_0^{lr}}{(1 + j\omega\tau)}. \tag{51}$$

The current on the tube is then

$$I_{sr} \simeq 2\pi a \sigma_{cn} E_0 = 2\pi E_0 \frac{2e^2 v_F \tau}{\pi^2 \hbar(1 + j\omega\tau)}, \tag{52}$$

for the small radius metallic tube, and

$$I_{lr} \simeq 2\pi a E_0 \frac{\tau e^2 2 \ln(2) k_B T}{\pi \hbar^2 (1 + j\omega\tau)}, \tag{53}$$

for the large radius tube, so that
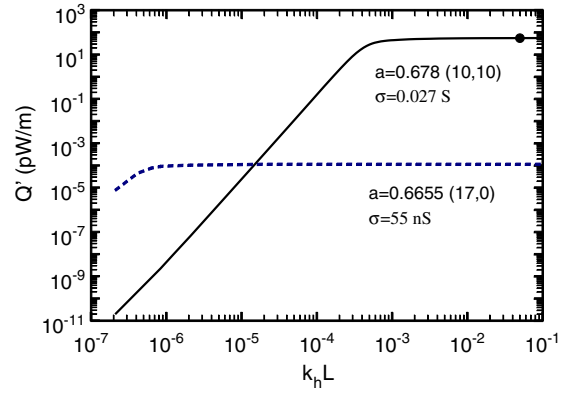


FIG. 6. (Color online) $Q' = Q/L$ (pW/m) from integral equation (21) with Eq. (59) for a (10,10) metallic SWCNT and for a (17,0) semiconducting SWCNT, for $E_0^i = 1$ V/m. The dot on the right side of the metallic tube curve is the predication based on the simple infinite-tube model (57).

$$Q'_{sr} = |E_0|^2 \frac{2e^2 v_F \tau}{\pi \hbar}, \tag{54}$$

$$Q'_{lr} = |E_0|^2 \frac{a\tau e^2 2 \ln(2) k_B T}{\hbar^2}. \tag{55}$$

With $\tau = 2a / \beta T$, where $\beta \sim 2 - 12$,[29]

$$Q'_{sr} = |E_0|^2 \frac{4e^2 a}{\hbar \beta} \left( \frac{v_F}{\pi T} \right), \tag{56}$$

$$Q'_{lr} = |E_0|^2 \frac{4e^2 a}{\hbar \beta} \left( \frac{a \ln(2) k_B}{\hbar} \right), \tag{57}$$

(for the large-radius tube, $\beta$ can be adjusted so that $\tau = \tau_{\mathrm{graphene}}$). These results are independent of frequency.

As with the electrically long solid cylinder, in both the small radius and large radius cases for an electrically long SWCNT, heating would be maximized if conductivity could be increased (see Fig. 6). For a (10,10) tube ($a = 0.678$ nm), if the tube is in air, $Q'_{sr}/|E_0|^2 = 0.05$ nW m/V$^2$, and, as a comparison, for a gold nanowire having $a = 10$ nm, $Q'/|E_0|^2 = 7.2$ nW m/V$^2$.

It is interesting to compare a hypothetical, single wall, large radius tube with a solid metal wire. For the tube,

$$Q'_{lr} = \frac{1}{2} |E_0|^2 \pi a^2 \left( \frac{8e^2}{\beta} \frac{\ln(2) k_B}{\pi \hbar^2} \right) = \frac{1}{2} |E_0|^2 \pi a^2 (0.47 \times 10^7), \tag{58}$$

using $\beta = 12$. For the wire, $Q' = \frac{1}{2} |E_0|^2 \pi a^2 \sigma$ from Eq. (19), and for copper and gold, $\sigma \sim 5 \times 10^7$, and so the solid wire and single wall of a large radius tube provide a similar level of power absorption $Q'$ (within one order of magnitude).

## G. Finite length SWCNT

To analyze a general, finite length CN we can use integral equation (21) if

$$z_s = \frac{1}{2\pi a \sigma_{cn}} \qquad (59)$$

is substituted for Eq. (24).[30] In that case, just as was found for solid cylinders, for short tubes where $k_h L \ll 1$ it is much better to have low conductivity. For example, for a (10,10) tube ($a = 0.678$ nm), assuming $L = 5$ $\mu$m in an air host at 10 MHz, $Q = 2.6 \times 10^{-26} |E_0|^2$ W, with an equivalent absorbing cross section of $1.9 \times 10^{-23}$ m$^2$. For a (17,0) zigzag tube, which is semiconducting (and thus has a much lower value of $\sigma$) but has approximately the same radius as the (10,10) metallic tube, $Q = 4.7 \times 10^{-22} |E_0|^2$ W, with an equivalent absorbing cross section of $3.5 \times 10^{-19}$ m$^2$. Thus, one can gain four orders of magnitude more heat from an electrically short semiconducting tube than from a metallic tube.

Figure 6 shows $Q' = Q/L$ (pW/m) determined from integral equation (21) with Eq. (59) for a (10,10) SWCNT, which is metallic and has relatively high conductivity ($\sigma_{cn} \simeq 0.027$ S), and for a (17,0) SWCNT, which is semiconducting and has a small conductivity ($\sigma_{cn} \simeq 5.5 \times 10^{-8}$ S). In both cases we assume $E_0^i = 1$ V/m. For electrically short tubes, the semiconducting tube is many orders of magnitude better for dissipating heat than the metallic tube, whereas for electrically long tubes the opposite occurs. This is consistent with the above findings for the solid, electrically long and electrically short cylinders. The dot on the right side of the metallic tube curve is the predication based on the simple infinite-tube model (56). As with the solid cylinder, because the speed of wave propagation on a SWCNT is much slower than on a macroscale metal tube due to kinetic inductance effects, the knee of the curve occurs at low values of $k_h L$ (for a macroradius wire, the transition from electrically short to electrically long would occur at $k_h L \sim 1$).

## III. HEATING OF NANOSPHERES AND COLLECTIONS OF NANOSPHERES

In this section, we consider heating of nanoparticles in an aqueous environment using classical heat conduction. Since the mean free path of heat carriers is on the angstrom level for liquids,[31] this should provide a reasonable approximation.[32] In support of this, molecular dynamics simulations have shown that the classical logarithmic diffusion of heat predicted by Eq. (5) for an infinite cylinder is valid for CNs in an octane liquid.[33]

The solution of the steady state heat (Poisson) Eq. (5) for a sphere subject to the boundary conditions of constant heat flux across the sphere-host medium interface, and a possible jump discontinuity in temperature due to a thermal contact resistance $R_c$ (m$^2$ K/W),[34]

$$q'' = -k_s \left. \frac{dT}{dr} \right|_{r=a^-} = -k_m \left. \frac{dT}{dr} \right|_{r=a^+}, \qquad (60)$$

$$T(a^-) - T(a^+) = q'' R_c, \qquad (61)$$

is

$$T(r) = \frac{S}{6k_s}(a^2 - r^2) + \frac{Sa^2}{3k_m} + \frac{SaR_c}{3} + T_\infty, \quad r < a \qquad (62)$$
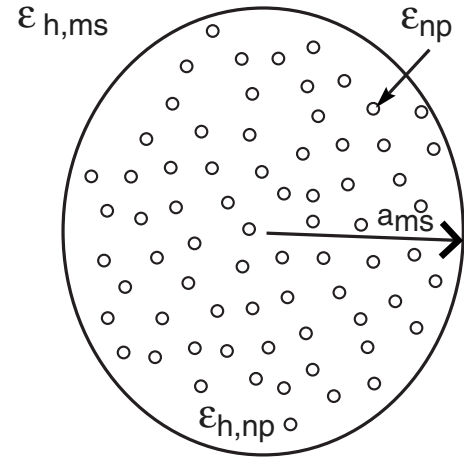


FIG. 7. A macroscale sphere of radius $a_{ms}$ containing a large collection of nanoparticles having permittivity $\varepsilon_{np}$. The nanoparticles are immersed in a host medium $\varepsilon_{h,np}$ and the single macrosphere is immersed in its host medium $\varepsilon_{h,ms}$.

$$= \frac{Sa^3}{3k_m} \frac{1}{r} + T_\infty = \frac{Q}{4\pi k_m} \frac{1}{r} + T_\infty, \quad r > a, \qquad (63)$$

where $S$ is the heat production density (W/m$^3$) and $T_\infty = T(r \to \infty)$. The thermal conductivities of the sphere and host materials are $k_s$ and $k_m$, respectively. The thermal contact resistance has been shown to be important for CNs,[33] although the situation is not clear for gold nanoparticles. The necessity of including $R_c$ would depend on the possible presence of a coating, however, the exterior temperature is independent of $R_c$. If we assume that the sphere is small and has large thermal conductivity, then we can approximate the sphere as an isothermal surface.

Heating of an individual spherical nanoparticle can be very small.[31] For example, assume an incident electromagnetic plane wave having $E_0 = 10$ kV/m in water ($\varepsilon_h = 70$), resulting in power density 110 W/cm$^2$. Even given this relatively large power density, assuming $f = 10$ MHz and a gold sphere having $a = 100$ nm, $C_a^{sph} = 2.6 \times 10^{-26}$ m$^2$ (dominated by the magnetic dipole moment), and $Q = 3 \times 10^{-20}$ W. The temperature on the sphere's outer surface with $k_m = 0.613$ W/mK for water is

$$\Delta T = T(a) - T_\infty = \frac{Q}{4\pi a k_m} \sim 10^{-14} \text{ K}. \qquad (64)$$

This is consistent with Ref. 31, where negligible heating was found for individual nanoparticles even assuming a much larger absorption cross section of $10^{-14}$ m$^2$ (which occurs at IR frequencies).

### A. Multiple particle heating

Using a large number of spherical nanoparticles, one can possibly obtain large temperature increases.[31,32] Consider a macroscale sphere of radius $a_{ms}$ containing a large collection of spherical nanoparticles having permittivity $\varepsilon_{np}$. The nanoparticles are immersed in a host medium $\varepsilon_{h,np}$ inside the macrosphere, and the macrosphere is immersed in its host medium $\varepsilon_{h,ms}$, as shown in Fig. 7. Although the macrosphere contains a large number of nanoparticles, it is still assumed

to be electrically small, such that $k_{h,\mathrm{ms}}a_{\mathrm{ms}} \ll 1$, consistent with test volumes considered in previous studies.[8,10,11]

Using Eq. (63) and assuming noninteracting, nonclumping nanoparticles,

$$\Delta T = \frac{Q}{4\pi a_{\mathrm{ms}} k_m} = \frac{Q_{\mathrm{np}} \rho_{\mathrm{np}} a_{\mathrm{ms}}^2}{3 k_m}, \qquad (65)$$

where $k_m$ is the thermal conductivity of the medium outside of the macrosphere, $Q = Q_{\mathrm{np}} \rho_{\mathrm{np}} 4\pi a_{\mathrm{ms}}^3 / 3$ is the total power dissipated in the macrosphere by all nanoparticles, $\rho_{\mathrm{np}}$ is the density of nanoparticles $(\mathrm{np}/\mathrm{m}^3)$, and

$$Q_{\mathrm{np}} = -k_{h,\mathrm{np}} I_a' \operatorname{Im}(\alpha_{\mathrm{np}}^e + \alpha_{\mathrm{np}}^m), \qquad (66)$$

is the energy deposited per nanoparticle (W/np) using Eq. (36). In Eq. (66), $I_a'$ is the intensity incident on the nanoparticles, which is different from the intensity incident on the macrosphere $I_a$ unless $\varepsilon_{h,\mathrm{ms}} = \varepsilon_{h,\mathrm{np}}$, and $\alpha_{\mathrm{np}}^{e,m}$ is the nanoparticle polarizability (bare or coated nanoparticles). Assuming a macrosphere volume of 5 ml, $a_{\mathrm{ms}} = 0.0106$ m, and an incident intensity $I_a' = 110$ W/cm$^2$, $\Delta T = Q_{\mathrm{np}} \rho_{\mathrm{np}} (6 \times 10^{-5})$. In order to obtain $\Delta T \sim 10$ K, we would need $Q_{\mathrm{np}} \rho_{\mathrm{np}} = 1.6 \times 10^5$ W/m$^3$. With 100 nm gold nanoparticles, since $Q_{\mathrm{np}} \sim 3 \times 10^{-20}$ W, this would require $\rho_{\mathrm{np}} \sim 10^{24}$ m$^{-3}$, which is not possible (volume fraction is greater than 1). As an alternative to Eq. (65), in the Appendix an effective medium formulation is presented.

In several recent papers greatly enhanced heating was obtained experimentally using nanoscale gold nanoparticles.[8–11] For example, in Ref. 8, 12.5–50 mg/l of 5 nm gold nanoparticles were used (corresponding to densities of $(1–5) \times 10^{18}$ m$^{-3}$) in cell cultures in a 60 mm Pyrex dish. In Ref. 10, 1.1–67 $\mu$mol/l of 5 nm gold nanoparticles in a 1 ml volume were used, corresponding to densities of $6.6 \times 10^{20} – 4 \times 10^{22}$ m$^{-3}$. In Ref. 11, 0.5 ml of 13 nm, citrate coated gold nanoparticles were used. Repeating the above analysis for $a = 5$ nm gold spheres in water $(\varepsilon_{h,\mathrm{np}} = 70)$, $Q_{\mathrm{np}} = 1.7 \times 10^{-26}$ W, the required density to produce an approximately 10 K change in temperature of the macrosphere would be $\rho_{\mathrm{np}} = 10^{29}$ m$^{-3}$, again, a nonphysical value. It seems likely that observed heating was due to particle clumping (this is evident in Ref. 8, but in Refs. 10 and 11 the nanoparticles seemed to be dispersed to some degree) or mutual particle interactions, or the presence of a coating on the nanoparticles (or some combination of these effects). As discussed above, the presence of a coating on a good conductor can increase the absorption cross section dramatically. For 5 nm gold particles with a coating having thickness $d = 0.1a$, $\varepsilon_{\mathrm{coat}}' = 4$, and $\sigma = 0.01$ S/m, $Q_{\mathrm{np}} = 2 \times 10^{-18}$ and the required particle density to yield a 10 K change in temperature of the macrosphere would be $\rho_{\mathrm{np}} \sim 8 \times 10^{22}$ m$^{-3}$ (volume fraction 0.04). For a 5 ml macrosphere, $\Delta T = 11.6$ K. Furthermore, since $\Delta T \propto a_{\mathrm{ms}}^2$, larger test volumes would increase the temperature substantially.

It should be noted that far-infrared absorption by metal particles has been a subject of debate,[35–45] since early measurements showed several orders of magnitude difference between theory and prediction in this frequency range. It has been shown that clustering/clumping of nanoparticles,[36–38,42] the presence of a resistive oxide coating,[35,36,38,39,41] and a
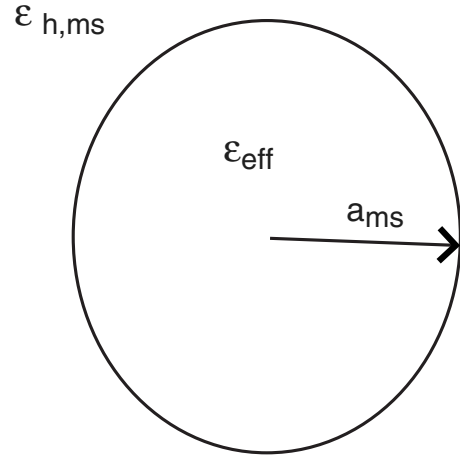


FIG. 8. The macrosphere in Fig. 7 is replaced with a homogeneous medium having effective permittivity $\varepsilon_{\mathrm{eff}}$.

combination of both effects can lead to dramatically enhanced absorption. For CNs, clumping and percolation effects are quite pronounced even at relatively low volume fractions,[46] although this subject is beyond the scope of the present work.

## IV. CONCLUSIONS

The enhancement of nanoparticle heating for applications such as thermoacoustic imaging and therapeutic heat delivery was considered. Simple equations were presented to determine the optimum material conductivity to maximize electromagnetic energy deposition in nanoparticles, including spheres, coated spheres, nanowires, and CNs. It was found that for electrically small particles, optimum heating occurs at relatively small conductivity values ($\sigma \ll 1$ S/m for spheres below 1 GHz, and $\sigma \ll 100$ S/m for cylinders). For electrically long wires at rf frequencies, it was found that the value of conductivity for maximum heating exceeds that of gold or copper for nanoscale radius values. Simple models indicate that recent measurements of temperature increases associated with gold nanoparticles in a host medium are probably due to a combination of clumping and coating.

## APPENDIX: EFFECTIVE MEDIUM MODEL

Alternative to Eq. (65), one can also consider the macrosphere containing nanoparticles as an effective medium, as depicted in Fig. 8. There is some convenience to this approach; however, as described below, the range of validity is somewhat limited.

Using the Maxwell–Garnett model generalized for the case of nanoparticles having both electric and magnetic polarizability in a general isotropic host medium,[47]

$$\varepsilon_{\mathrm{eff}} = \varepsilon_{h,\mathrm{np}} \frac{3 + 2\rho_{\mathrm{np}}\alpha_{\mathrm{np}}^e}{3 - \rho_{\mathrm{np}}\alpha_{\mathrm{np}}^e},$$

$$\mu_{\mathrm{eff}} = \mu_{h,\mathrm{np}} \frac{3 + 2\rho_{\mathrm{np}}\alpha_{\mathrm{np}}^m}{3 - \rho_{\mathrm{np}}\alpha_{\mathrm{np}}^m}, \qquad (A1)$$

where the electric and magnetic polarizability $\alpha^e$ and $\alpha^m$ are for bare or coated nanoparticles, and $\varepsilon_{h,\mathrm{np}}$, $\mu_{h,\mathrm{np}}$ characterize

the host medium. We assume spherical nanoparticles, $\mu_{h,np}$ $=1$, and that the nanoparticles are nonmagnetic, so that the magnetic dipole moment is due to eddy currents [and so, from Eq. (36), $\mu_{eff}$ depends on particle size, and not just on volume fraction]. The absorption cross section for the effective medium macrosphere is

$$C_a^{eff} = -k_{h,ms} 4\pi a_{ms}^3 \left[ \text{Im}\left( \frac{\varepsilon_{eff} - \varepsilon_{h,ms}}{\varepsilon_{eff} + 2\varepsilon_{h,ms}} \right) \right.$$
$$\left. + \text{Im}\left( \frac{\mu_{eff} - \mu_{h,ms}}{\mu_{eff} + 2\mu_{h,ms}} \right) \right], \tag{A2}$$

and with $Q^{eff} = C_a^{eff} I_a$, Eq. (63) for a single macrosphere leads to

$$\Delta T = \frac{Q^{eff}}{4\pi a_{ms} k_m} = \frac{-k_{h,ms} a_{ms}^2 I_a}{k_m} \left[ \text{Im}\left( \frac{\varepsilon_{eff} - \varepsilon_{h,ms}}{\varepsilon_{eff} + 2\varepsilon_{h,ms}} \right) \right.$$
$$\left. + \text{Im}\left( \frac{\mu_{eff} - \mu_{h,ms}}{\mu_{eff} + 2\mu_{h,ms}} \right) \right], \tag{A3}$$

where $k_m$ is the thermal conductivity outside the macrosphere. It is interesting to note that if $\varepsilon_{h,np} = \varepsilon_{h,ms}$ and $\mu_{h,ms} = 1$, then $I_a = I_a'$ and Eqs. (A3) and (65) are equivalent. In this case, we can model the macrosphere as a collection of nanoparticles using Eq. (65), or as one region having effective properties using Eq. (A3). However, for $\varepsilon_{h,np} \neq \varepsilon_{h,ms} (I_a \neq I_a')$ the expressions (A3) and (65) are not equivalent, but yield numerically similar results when the electric dipole contribution is dominant and the particle density $\rho_{np}$ is small (e.g., volume fraction less than 0.1). In this case $I_a' = |\mathbf{E}_{np}|^2 / 2\sqrt{\mu_0/\varepsilon_0 \varepsilon_{h,np}}$, where

$$\mathbf{E}_{np} = \frac{3\varepsilon_{h,ms}}{\varepsilon_{h,np} + 2\varepsilon_{h,ms}} \mathbf{E}_{ms}, \tag{A4}$$

is the field inside the macrosphere (i.e., the field incident on the nanoparticles) and $\mathbf{E}_{ms}$ is the field incident on the macrosphere. As discussed in Refs. 48 and 49, absorption and heating can be computed via a quasistatic effective permittivity $\varepsilon_{eff}$ [e.g., as in Eq. (A1)], but not, in general, by extended effective medium theories (e.g., extended to higher frequencies, or generally when the effective parameters become particle size-dependent, rather than simply dependent on the volume fraction). A clear manifestation of this problem is that one may obtain an imaginary part of the effective parameters as particle size increases even for nonabsorbing host and inclusions, which models an increase in scattering. Therefore, extended effective medium theories may be useful for computing extinction, but not for absorption.

[1] L. Nie, D. Xing, D. Yang, and L. Zeng, Proceedings of the IEEE-ICME Int. Conf., 2007 (unpublished), p. 989.
[2] M. Pramanik, M. Swierczewska, D. Green, B. Sitharaman, and L. V. Wang, J. Biomed. Opt. **14**, 034018 (2009).
[3] A. de la Zerda, C. Zavaleta, S. Keren, S. Vaithilingam, S. Bodapati, Z. Liu, J. Levi, B. R. Smith, T. J. Ma, O. Oralkan, Z. Cheng, X. Chen, H. Dai, B. T. Khuri-Yakub, and S. S. Gambhi, Nat. Nanotechnol. **3**, 557 (2008).
[4] T. Bowen, Ultrasonics Symposium, July 1981 (unpublished).
[5] R. A. Kruger, K. K. Kopecky, A. M. Aisen, D. R. Reinecke, G. A. Kruger, and W. L. Kiser, Jr., Radiology **211**, 275 (1999).
[6] M. Xu and L. V. Wang, Rev. Sci. Instrum. **77**, 041101 (2006).
[7] D. Fallon, L. Yan, G. W. Hanson, and S. K. Patch, Rev. Sci. Instrum. **80**, 064301 (2009).
[8] S. A. Curley, P. Cherukuri, K. Briggs, C. R. Patra, M. Upton, E. Dolson, and P. Mukherjee, J. Exp. Ther. Oncol. **7**, 313 (2008).
[9] C. J. Gannon, P. Cherukuri, B. I. Yakobson, L. Cognet, J. S. Kanzius, C. Kittrell, R. B. Weisman, M. Pasquali, H. K. Schmidt, R. E. Smalley, and S. A. Curley, Cancer **110**, 2654 (2007).
[10] C. J. Gannon, C. R. Patra, R. Bhattacharya, P. Mukherjee, and S. A. Curley, Nanobiotechnology **6**, 2 (2008).
[11] J. Cardinal, J. Klune, E. Chory, G. Jeyabalan, J. Kanzius, M. Nalesnik, and D. Geller, Surgery **144**, 125 (2008).
[12] N. W. S. Kam, M. O'Connell, J. A. Wisdom, and H. Dai, Proc. Natl. Acad. Sci. U.S.A. **102**, 11600 (2005).
[13] M. D. Arnold and M. G. Blaber, Opt. Express **17**, 3835 (2009).
[14] M. G. Blaber, N. Harris, M. J. Ford, and M. B. Cortie, in International Conference on Nanoscience and Nanotechnology, ICONN '06, 3–7 July 2006, Brisbane, Qld. (IEEE, New York, 2006), p. 556.
[15] L. D. Landau, E. M. Lifshitz, and L. P. Pitaevskii, *Electrodynamics of Continuous Media*, 2nd ed. (Elsevier, Amsterdam, 1984).
[16] E. J. Rothwell and M. J. Cloud, *Electromagnetics*, 2nd ed. (CRC, Boca Raton, 2008).
[17] R. F. Harrington, *Time-Harmonic Electromagnetic Fields* (Wiley, New York, 1961).
[18] R. W. P. King and T. T. Wu, IEEE Trans. Antennas Propag. **AP-14**, 524 (1966).
[19] T. T. Wu, in *Antenna Theory*, edited by R. E. Collin and F. J. Zucker (McGraw-Hill, New York, 1969), Chap. 8.
[20] E. Hallén, *Electromagnetic Theory* (Wiley, New York, 1962).
[21] J. A. Stratton, *Electromagnetic Theory* (McGraw-Hill, New York, 1941).
[22] R. F. Harrington, *Field Computation by Moment Methods* (Krieger, Melbourne, FL, 1968).
[23] C. F. Bohren and D. R. Huffman, *Absorption and Scattering of Light by Small Particles* (Wiley, New York, 1983).
[24] G. W. Hanson, IEEE Trans. Antennas Propag. **54**, 3677 (2006).
[25] P.-O. Chapuis, M. Laroche, S. Volz, and J.-J. Greffet, Phys. Rev. B **77**, 125402 (2008).
[26] S. M. Mikki and A. A. Kishk, Microwave Opt. Technol. Lett. **49**, 2360 (2007).
[27] G. Ya. Slepyan, S. A. Maksimenko, A. Lakhtakia, O. Yevtushenko, and A. V. Gusakov, Phys. Rev. B **60**, 17136 (1999).
[28] S. A. Maksimenko and G. Y. Slepyan, in *Electromagnetic Fields in Unconventional Materials and Structures*, edited by O. N. Singh and A. Lakhtakia (Wiley, New York, 2000).
[29] X. Zhou, J.-Y. Park, S. Huang, J. Liu, and P. L. McEuen, Phys. Rev. Lett. **95**, 146805 (2005).
[30] G. W. Hanson, IEEE Trans. Antennas Propag. **53**, 3426 (2005).
[31] P. Keblinski, D. G. Cahill, A. Bodapati, C. R. Sullivan, and T. A. Taton, J. Appl. Phys. **100**, 054305 (2006).
[32] C. T. Avedisian, R. E. Cavicchi, P. L. McEuen, and X. Zhou, Proceedings of the ITP2007, Bansko, Bulgaria, 2007 (unpublished).
[33] S. Shenogin, L. Xue, R. Ozisik, P. Keblinski, and D. G. Cahill, J. Appl. Phys. **95**, 8136 (2004).
[34] F. Kreith and W. Z. Black, *Basic Heat Transfer* (Harper, New York, 1980).
[35] E. Šimánek, Phys. Rev. Lett. **38**, 1161 (1977).
[36] R. Ruppin, Phys. Rev. B **19**, 1318 (1979).
[37] N. E. Russell, J. C. Garland, and D. B. Tanner, Phys. Rev. B **23**, 632 (1981).
[38] P. N. Sen and D. B. Tanner, Phys. Rev. B **26**, 3582 (1982).
[39] S.-I. Lee, T. W. Noh, and J. R. Gaines, Phys. Rev. B **32**, 3580 (1985).
[40] W. A. Curtin and N. W. Ashcroft, Phys. Rev. B **31**, 3287 (1985).
[41] S.-I. Lee, T. W. Noh, K. Cummings, and J. R. Gaines, Phys. Rev. Lett. **55**, 1626 (1985).
[42] R. Fuchs, Phys. Rev. B **35**, 7700 (1987).
[43] Y. H. Kim and D. B. Tanner, Phys. Rev. B **39**, 3585 (1989).
[44] R. P. Devaty and A. J. Sievers, Phys. Rev. B **41**, 7421 (1990).
[45] A. V. Plyukhin, A. K. Sarychev, and A. M. Dykhne, Phys. Rev. B **59**, 1685 (1999).
[46] K. R. Paton and A. H. Windle, Carbon **46**, 1935 (2008).
[47] I. V. Lindell, A. H. Sihvola, S. A. Tretyakov, and A. J. Viitanen, *Electromagnetic Waves in Chiral and Bi-Isotropic Media* (Artech House, Boston, 1994).
[48] C. F. Bohren, J. Atmos. Sci. **43**, 468 (1986).
[49] R. Ruppin, Opt. Commun. **182**, 273 (2000).